Calculation of high-order wave loads on a vertical circular cylinder using the SWENSE method

Zhaobin Li*, Lionel Gentaz, Guillaume Ducrozet, Pierre Ferrant
LHEEA Lab, Ecole Centrale de Nantes, CNRS UMR 6598, France
zhaobin.li@ec-nantes.fr

1 Introduction

The ringing phenomenon is associated to the excitation of a structure at its natural frequency through higher harmonic components of the wave loading. Observations of this phenomenon on model tests were reported first at the beginning of the 90's, before being observed at full scale during storm events in the North Sea. As the corresponding loading may induce a significant increase of the fatigue of the structure, the discovery of the phenomenon triggered strong research efforts for the understanding and prediction of higher harmonic wave loads on offshore structures. Using potential flow theory, Faltinsen et al (1995) developed a third order perturbation theory in the long wave regime. Malenica & Molin (M&M) (1995) proposed a complete third order quasi-analytical solution for the triple harmonic force component on a vertical cylinder in regular waves. Ferrant (1996) used a time domain fully nonlinear boundary element method and obtained results in good agreement with the M&M's theory. Huseby and Grue (1998) reported experiments on a bottom-mounted vertical cylinder in deep water conditions, focusing on the third harmonic force components, and confirming again the validity of M&M formulation. The confrontation of these experimental data to results of fully nonlinear potential flow simulations leads to favorable comparisons up to the seventh harmonic force components, published in Ferrant (1998) and Huseby & Grue (2000).

In the present paper, we are revisiting this set of data, using the so-called SWENSE method in which the flow is decomposed into an incident wave system modelled by fully nonlinear potential flow theory, and a diffracted/radiated flow solved using a modified version of Navier-Stokes equations in which incident flow components appear as forcing terms. The main finding is that the inclusion of viscous effects leads to a slightly better agreement with experiments for the wave frequency component, compared to potential flow results. A first analysis seems to indicate that the observed deviation between potential flow and viscous flow results is due to the influence of a minor flow detachment on the pressure component of the load, while the frictional component have little influence.

2 Numerical method

The SWENSE method divided the problem of wave-structure interaction into two parts: (1) incident part takes into account the wave propagation in the whole computational domain, where the solution is directly given by potential wave theory; (2) diffracted part serves as a correction to the incident part due to the presence of body in the wave and the viscosity. The decomposition is shown by Eqn.1 where the total variable χ_T is divided into the variable of incident wave χ_I and the variable of diffracted field χ_D. χ_I is explicitly known from potential wave theory, thus only the diffracted variable χ_D needs to be calculated by CFD. This decomposition method is first suggested by Ferrant et al (2003) and developed and validated by Gentaz et al (2004) in a finite differences code Icare-Swense using the free surface tracking method.

$$\chi_T = \chi_I + \chi_D \tag{1}$$

Applying the decomposition method on the velocity $\mathbf{u_T} = \mathbf{u_I} + \mathbf{u_D}$, pressure $p = p_I + p_D$ and the free surface elevation $h_T = h_I + h_D$, and using ν_e for the effective viscosity, the Navier-Stokes equations and the free surface tracking equation can be transformed into:

$$\nabla \bullet \mathbf{u_D} = 0 \tag{2}$$

$$\frac{\partial \mathbf{u_D}}{\partial t} + \nabla \bullet (\mathbf{u_T u_D}) - \nabla \bullet (\nu_e \nabla \mathbf{u_D}) = -\nabla \bullet (\mathbf{u_D u_I}) + \nabla \bullet (\nu_e \nabla \mathbf{u_I}) - \frac{1}{\rho} \nabla p_D \tag{3}$$

$$\frac{\partial h_D}{\partial t} + u_T \frac{\partial h_D}{\partial x} + v_T \frac{\partial h_D}{\partial y} - w_T = -\frac{\partial h_I}{\partial t} - u_T \frac{\partial h_I}{\partial x} - v_T \frac{\partial h_I}{\partial y} \tag{4}$$

The benefits of the SWENSE decomposition are: (1) accuracy of the incident wave propagation: as the incident variables are explicitly obtained by wave theories, the quality of the CFD results does not influence the incident wave; (2) efficiency: the diffracted field only need to be calculated accurately near the offshore structure, so we can use fine meshes close to the structure and coarse meshes far away from the body; (3) simplicity of the far field boundary condition: as the wave is disturbed only in the vicinity of the structure, the boundary conditions for the diffracted variables are set to be zero in the far field.

3 Simulation setup

In this study we consider a bottom-mounted surface piercing vertical circular cylinder in regular waves. The radius of the cylinder is R=0.03m, the water depth is h=0.6m, the wave is defined such as its wave number k satisfies kR=0.245. A series of simulations is carried out with 8 different wave amplitudes a defined by ka=[0.06, 0.08, 0.10, 0.13, 015, 0.17, 0.20, 0.24]. The same cases have been studied experimentally by Huseby and Grue (2000) and numerically by Ferrant (1998) and Shao and Faltinsen (2014). In contrary to the assumption of potential flow used in previous studies, we consider the viscosity of the water and applied the no-slip condition on the cylinder. For the steepest wave, the maximum Reynolds number calculated based on the diameter of the cylinder and the maximum wave velocity is $Re = 1.55 \times 10^4$ and the maximum Keulegen-Carpenter number is $KC = 3.01$, indicating the flow is likely to oscillate between laminar and transitional regimes during the wave excitation cycles. The strategy adopted here with respect to this relatively low Reynolds number problem is a direct modeling of the viscous stresses of the Navier-Stokes equations (no turbulence model), with a care paid to the mesh size so as to capture as best the viscous effects in the vicinity of the body (boundary layer and flow detached areas).

The simulations are carried out by the in-house monophase finite difference CFD code Icare-swense. The regular wave is generated by the stream function theory. A structured cylindrical mesh is used (see Fig.1). The domain's radius is 4 meters, which is approximately equal to 5 times the wave length. In the radial direction the domain is discretized into 128 grids, the minimum grid size being 6×10^{-6}m close to the cylinder to capture the large velocity gradient, and 1 meter on the far field boundary. The large grid size is intentionally applied to absorb the diffracted waves. In the tangential direction, half of the domain is evenly discretized into 80 grids using the symmetric assumption. Along the vertical axis, the domain is discretized into 60 grids and the mesh is gradually refined near the free surface. All the simulations are ran for 16 wave periods with 100 time steps per wave period. The start time t=0 is defined as the incident wave crest locates at the center line of the cylinder. The wave amplitude gradually increases from 0 to its target value a in the first period.

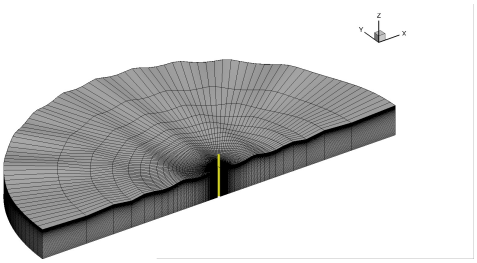

Figure 1: Computational grid used in Icare-swense

4 Numerical results

During the simulation, the time history of the horizontal force on the cylinder is firstly recorded and the value from the 6 to 15 wave period is used for Fourier analysis where steady state has been achieved. The amplitude of high-order wave force F_n is non-dimensinalized by $F_n' = F_n/(\rho g R^3 \cdot (A/R)^n)$. In Fig.2, the first to fourth harmonic non-dimensional force's amplitude and their phase shift are presented with a comparison to the results of Shao et al (2014), Ferrant (1998), the experiment data of Huseby and Grue (2000), and the analytical solution from Malenica and Molin (1995) which is represented by the bold dash line.

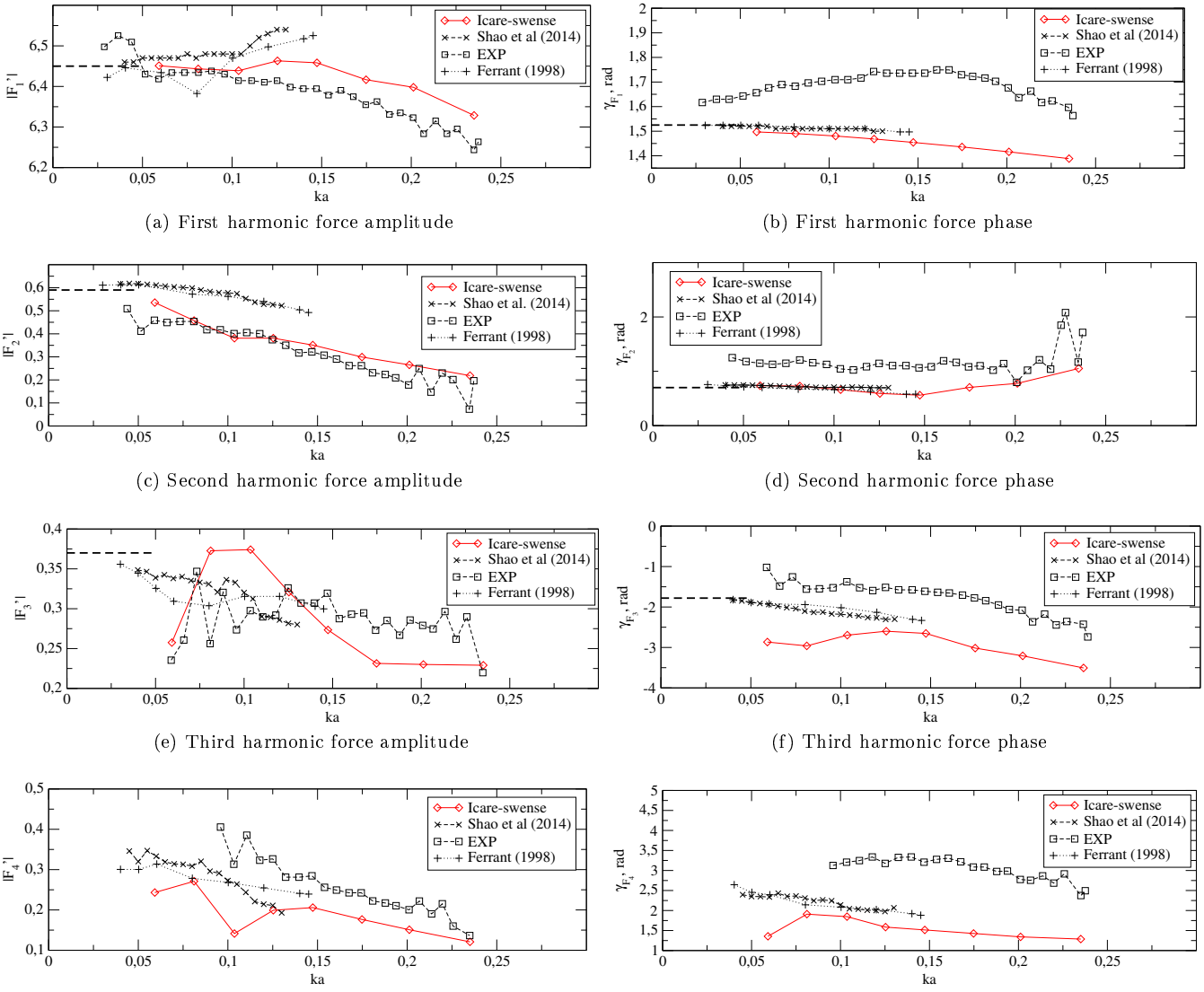

(a) First harmonic force amplitude

(b) First harmonic force phase

(c) Second harmonic force amplitude

(d) Second harmonic force phase

(e) Third harmonic force amplitude

(f) Third harmonic force phase

(g) Fourth harmonic force amplitude

(h) Fourth harmonic force phase

Figure 2: Comparison of the first to fourth harmonics of horizontal forces on vertical circular cylinder in regular waves with kR=0.245.

5 Discussion and future work

Results from both fully nonlinear models of Ferrant (1998) and Shao & Faltinsen (2014) are in good agreement for all the components, and close to experimental results.

The numerical results obtained by the SWENSE method are in good agreement with the experimental data, especially for the first and second harmonic components. For third and fourth harmonic components, slight differences are observed between potential flow and viscous flow results, although the agreement with experiments is similar. Results from M&M's theory, asymptotically valid in the zero steepness limit for an inviscid fluid are indicated by the bold dashed lines. We observe that the three sets of nonlinear numerical results converge to these limit values when the wave amplitude decreases. When the amplitude is increased, potential flow solvers have difficulties in simulating cases above ka=0.13-0.15, due to instabilities at the free surface, while the viscous flow solver, although base on a free surface tracking scheme, is able to cover the whole amplitude range, up to ka=0.24.

In Fig.2a (first harmonic amplitude), we can observe that above ka=0.1, potential flow results tend to deviate from experimental results, while results obtained with the viscous flow solver, although showing a slight deviation, tend to remain closer to the experiments. The analysis of the pressure and friction terms in the fluid load show that the friction term remains negligible, and then that the source of the difference between potential flow and viscous flow solution appears mainly through the pressure. A possible explanation lies in flow separation initiated by viscous effects in the boundary layer, as exemplified by Fig.3 showing small separated flow areas appearing downwave when a crest is passing, and upwave in the troughs.

We are now running convergence tests in order to be able to confirm this analysis. Full results will be presented at the workshop.

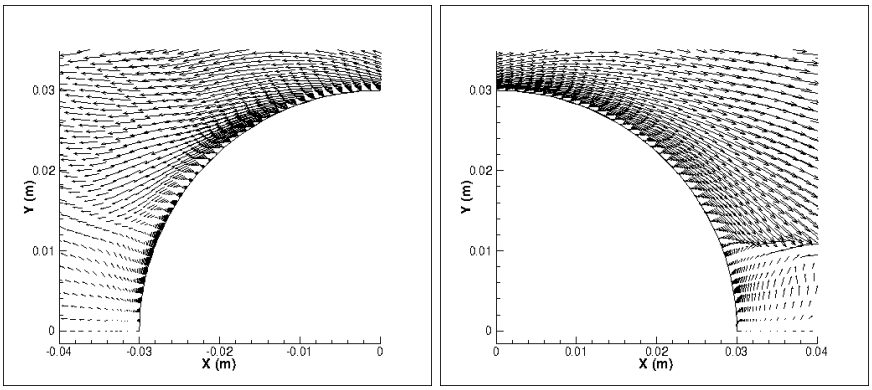

(a) t=8.5T (b) t=9T

Figure 3: Flow separation on the cylinder for wave steepness $ka = 0.24$. The velocity vector field is plotted on the free surface. (a) In wave trough, zoom in on the upstream side of the cylinder. (b) In wave crest, zoom in on the downstream side of the cylinder.

Acknowledgement

The first author acknowledges the financial support from China Scholarship Council (CSC) for his PhD study.

References

W Bai and R Eatock Taylor. Numerical simulation of fully nonlinear regular and focused wave diffraction around a vertical cylinder using domain decomposition. *Applied Ocean Research*, 29(1):55–71, 2007.

OM Faltinsen, JN Newman, and T Vinje. Nonlinear wave loads on a slender vertical cylinder. *Journal of Fluid Mechanics*, 289: 179–198, 1995.

P Ferrant. Computation of higher order diffraction effects using a fully nonlinear simulation method. *Proc. 11th International Workshop on Water Waves and Floating Bodies, Hamburg*, 1996.

Pierre Ferrant. Fully nonlinear interactions of long-crested wave packets with a three dimensional body. In *Proc. 22nd ONR Symposium on Naval Hydrodynamics*, pages 403–415, 1998.

Pierre Ferrant, Lionel Gentaz, Bertrand Alessandrini, and David Le Touzé. A potential/ranse approach for regular water wave diffraction about 2-d structures. *Ship Technology Research*, 50(4):165–171, 2003.

L Gentaz, R Luquet, B Alessandrini, and P Ferrant. Numerical simulation of the 3d viscous flow around a vertical cylinder in non-linear waves using an explicit incident wave model. In *ASME 2004 23rd International Conference on Offshore Mechanics and Arctic Engineering*, pages 157–163. American Society of Mechanical Engineers, 2004.

Morten Huseby and John Grue. An experimental investigation of higher harmonic forces on a vertical cylinder in long waves. In *Proc. 13th International Workshop on Water Waves and Floating Bodies, Alphen aan den Rijn (ed. AJ Hermans)*, pages 43–46, 1998.

Morten Huseby and John Grue. An experimental investigation of higher-harmonic wave forces on a vertical cylinder. *Journal of fluid Mechanics*, 414:75–103, 2000.

Šime Malenica and B Molin. Third-harmonic wave diffraction by a vertical cylinder. *Journal of Fluid Mechanics*, 302:203–229, 1995.

Bo T Paulsen, Henrik Bredmose, Harry B Bingham, and Niels Gjøl Jacobsen. Forcing of a bottom-mounted circular cylinder by steep regular water waves at finite depth. *Journal of Fluid Mechanics*, 755:1–34, 2014.

Yan-Lin Shao and Odd M Faltinsen. A harmonic polynomial cell (hpc) method for 3d laplace equation with application in marine hydrodynamics. *Journal of Computational Physics*, 274:312–332, 2014.